Chemical Science

ROYAL SOCIETY OF CHEMISTRY

EDGE ARTICLE

View Article Online
View Journal | View Issue

Cite this: *Chem. Sci.*, 2020, **11**, 12695

All publication charges for this article have been paid for by the Royal Society of Chemistry

Received 8th May 2020
Accepted 14th July 2020

DOI: 10.1039/d0sc02623a

rsc.li/chemical-science

A new pentacyclic pyrylium fluorescent probe that responds to pH imbalance during apoptosis†

Sandip Chakraborty,[ab] Manu M. Joseph,[a] Sunil Varughese,[ab] Samrat Ghosh,[a] Kaustabh K. Maiti,[ab] Animesh Samanta *[ac] and Ayyappanpillai Ajayaghosh *[ab]

Efficient fluorophores with easy synthetic routes and fast responses are of great importance in clinical diagnostics. Herein, we report a new, rigid pentacyclic pyrylium fluorophore, **PS-OMe**, synthesised in a single step by a modified Vilsmeier–Haack reaction. Insights into the reaction mechanism facilitated a new reaction protocol for the efficient synthesis of **PS-OMe** which upon demethylation resulted in a "turn-on" pH sensor, **PS-OH**. This new fluorescent probe has been successfully used to monitor intracellular acidification at physiological pH. From the fluorescence image analysis, we were able to quantify the intracellular dynamic pH change during apoptosis. This new pH probe is a potential chemical tool for screening, drug discovery and dose determination in cancer therapy.

Introduction

Molecular probes that serve as an effective tool for imaging biological tissues and cells play an important role in disease diagnostics and treatment modalities.[1,2] Over a period of time, a large number of fluorescent probes have been developed for various analyte sensing and imaging applications. However, most of these probes are essentially derived from 'core scaffolds' such as squaraine, rhodamine, coumarin, BODIPY *etc.* In this context, developing a new core scaffold with easy synthesis, high yield, and good photophysical properties, stability and biocompatibility is of paramount importance. This may set up a platform for developing new probes with novel sets of advantages for sensing and imaging of cells and tissues for disease diagnosis and therapy.[3]

Imaging of pH variations in cells is important for proper diagnosis of several types of cancers. The imbalance of pH in cancerous cells during apoptosis caused by chemotherapy needs to be monitored in real time for post treatment wellness of patients.[4] The extent of pH decrease provides insights into the effectiveness of therapeutic agents, pathways, doses and time needed for apoptosis.[5] Owing to the significant roles of pH in many physiological processes within intracellular organelles, enormous efforts have been made for the development of new pH imaging chemical probes with improved optical properties.[6,7] The imbalance of functional pH within cellular microenvironments is also associated with dysfunctions of enzymes and cellular events. For example, variations of the cytosolic pH are closely associated with cell migration, cellular proliferation and apoptosis. It is evident that extracellular acidic pH is highly favourable for regular growth of cancer cells and metastasis of tumours.[8] Thus, accurate measurement of pH imbalance in cells is of paramount importance in clinical analysis and disease diagnostics.

Considering its advantages in terms of high sensitivity, simplicity, real-time monitoring, applicability to microenvironments and non-invasive detection with high spatiotemporal resolution, fluorescent imaging is now in the forefront as a diagnostic tool.[9,10] Fluorescent probes based on organic small molecules are particularly preferred owing to their biocompatibility, solubility and ease of synthetic modifications.[11]

'Turn-on' pH probes have gained attention as they can easily discriminate between "on–off" states during the imbalance of pH. Several "off–on" probes are reported in the literature; however, majority of them have limited use due to difficult synthetic access,[12] poor solubility and partial or strong background fluorescence at physiological pH. Therefore, new fluorescent probes which are easily accessible and highly stable with bright fluorescence are necessary for the advancement of biological imaging and diagnostic applications. Pyrylium derivatives are known as highly fluorescent chromophores, used for a wide range of applications.[13–15] Herein, we report a modified Vilsmeier–Haack reaction for the synthesis of a pentacyclic pyrylium fluorophore **PS-OMe** which is a precursor of a turn-on fluorescent probe **PS-OH**. A mechanistic

[a]*Chemical Sciences and Technology Division, CSIR-National Institute for Interdisciplinary Science and Technology (CSIR-NIIST), Thiruvananthapuram 695 019, India. E-mail: ajayaghosh@niist.res.in*

[b]*Academy of Scientific and Innovative Research (AcSIR), CSIR – Human Resource Development Centre, Ghaziabad 201002, India*

[c]*Department of Chemistry, Shiv Nadar University, NH91, Dadri, Gautam Buddh Nagar, 201314, India. E-mail: animesh.samanta@snu.edu.in*

† Electronic supplementary information (ESI) available: Experimental details, synthesis procedures and characterization data of the compounds, and additional figures. CCDC 1985212. For ESI and crystallographic data in CIF or other electronic format see DOI: 10.1039/d0sc02623a

understanding of the synthesis of **PS-OMe** resulted in an alternate efficient route for its synthesis and subsequent demethylation to **PS-OH**. We further describe the use of the new probe for the real time monitoring of pH imbalance during chemotherapy or apoptosis by the fluorescence 'on–off' technique.

Results and discussion

Design and synthesis of the pyrylium fluorophore

The main points considered for the design of the new probe were (i) a simple synthetic strategy to produce an efficient fluorescent probe for pH detection, (ii) to monitor intracellular pH (pH_i) imbalance during apoptotic cellular dysfunction by fluorescence variation and (iii) the real time monitoring of dynamic pH change during the treatment of cells with apoptotic reagents or anticancer drugs. We hypothesized that this approach may provide a unique opportunity to develop an effective sensor to monitor pH imbalance during apoptosis. To achieve these objectives, we have designed a new synthetic protocol for the preparation of the fluorescent pyrylium derivative **PS-OH**, using the modified Vilsmeier–Haack reaction. As illustrated in Scheme 1, we started with 6-methoxy tetralone which is a key intermediate for many heterocyclic syntheses with diverse pharmacological properties. The Vilsmeier–Haack formylation reaction of 6-methoxy tetralone (**1**) at 80 °C produces a reactive 1-chloro-6-methoxy-3,4-dihydronaphthalene-2-carbaldehyde (**T-CHO**) when dimethyl formamide (DMF) and phosphorus oxychloride ($POCl_3$) were premixed to obtain the Vilsmeier–Haack iminium salts (*N*-(chloromethylene)-*N*-methylmethanaminium). In contrast, dropwise addition of $POCl_3$ to 6-methoxytetralone in DMF at 80 °C led to an additional product of 4-chloro-1,2-dihydro-7-methoxy-naphthalene (**T-Cl**) along with **T-CHO**. It is noted that if Vilsmeier–Haack iminium salts are not prepared through a premixed protocol, the formylation reaction is suppressed. In contrast, here a part of 6-methoxy tetralone reacts directly with $POCl_3$ to render a reactive intermediate (**T-Cl**) along with the expected **T-CHO** regardless of the reaction temperature. However, a high temperature (80 °C) leads to better yield (~35%) of **T-Cl** compare to the previous reports[16,17] (Scheme 1).

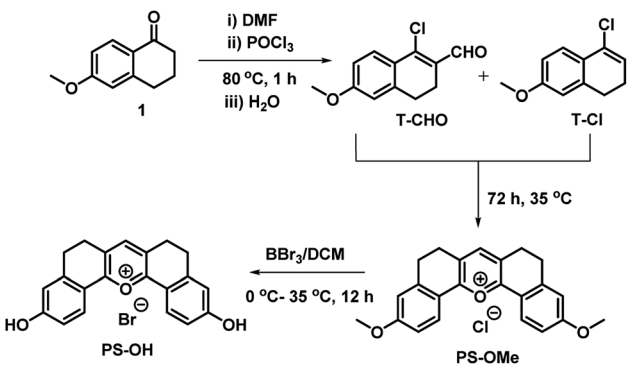

Scheme 1 The modified Vilsmeier–Haack synthesis of the symmetrical pyrylium dye, **PS-OMe**, leading to the fluorescent probe **PS-OH** by demethylation using BBr_3.

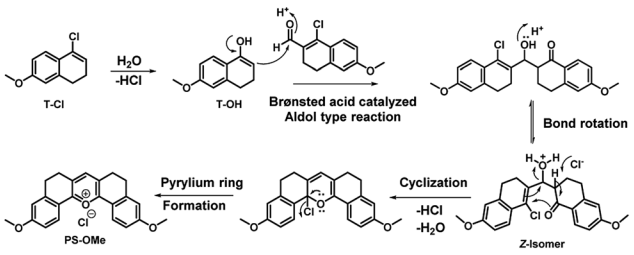

Fig. 1 Possible mechanism of formation of **PS-OMe**.

Interestingly, when the concentrated ethyl acetate extract of the reaction mixture was kept in the ambient atmosphere, a bright yellow fluorescence emitting fluorophore was formed. This serendipitous observation revealed that, the vinyl chloride of **T-Cl** was hydrolysed in contact with moisture to form an unstable enol, **T-OH** (Fig. 1) which undergoes cyclo-condensation with **T-CHO** to provide a pentacyclic symmetric pyrylium fluorophore named **PS-OMe**. To confirm the reaction pathway, firstly, the isolated compounds (**T-CHO**, **T-Cl**) were mixed and kept under inert conditions; however, we could not observe the formation of the pyrylium fluorophore even after one week. The proposed mechanism of **PS-OMe** formation is in good agreement with previous reports which suggest that the vinyl chloro functional group is the one which is labile towards nucleophiles.[18,19] **PS-OMe** was isolated by column-chromatography over silica gel using 6% methanol in chloroform as the eluent in 28% yield. To confirm the reaction pathway in the second step of the mechanism, we chose a few catalysts including Brønsted and Lewis acids since the proposed mechanism (Fig. 1) involved aldol type condensation. Hence, we performed acid catalysed condensation of isolated **T-CHO** and 6-methoxy tetralone in the presence of Brønsted and Lewis acids (Scheme 2). $AlCl_3$ was found to be the best acid catalyst (~70%) followed by triflic acid (~61%) among other catalysts. The results are summarized in Table 1.

PS-OMe is composed of a donor–acceptor–donor (D–A–D) system where the highly electron deficient pyrylium ring acts as a good acceptor and the corresponding two anisole rings connected to the 2 and 6 positions of the pyrylium ring act as strong donors. Furthermore, the six membered bridges play a crucial role in improving rigidity of the structure to enhance the fluorescence quantum efficiency. The fluorescent probe **PS-OH** was obtained by the demethylation of **PS-OMe** by treating with boron tribromide (Scheme 1). All new products

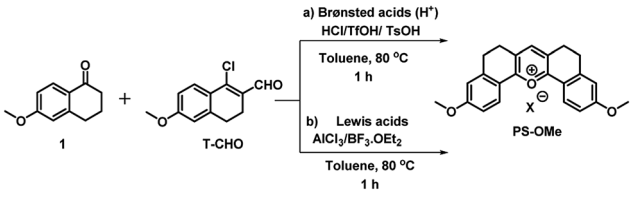

Scheme 2 A new alternate synthesis of the pentacyclic symmetrical pyrylium dye, **PS-OMe**, using (a) Brønsted acid (H^+) and (b) Lewis acid catalysts.

Table 1 Synthesis of **PS-OMe** with different Brønsted and Lewis acid catalysts[a]

Entry	Catalyst/equiv.	Time/h	Temp./°C	Yield[b]/%
1	HCl (1)	12	80	15
2	TFA (1)	12	80	n.d.
3	TFOH (0.3)	1	80	61
4	PSOH (0.3)	1	80	29
5	$BF_3 \cdot OEt_2$ (0.1)	1	80	51
6	$AlCl_3$ (0.1)	1	80	70

[a] Conditions: reaction of 6-methoxy tetralone (1.0 mmol) and **T-CHO** (1.0 mmol) using different catalysts in toluene at 80 °C. [b] Isolated yield.

obtained were characterized by various spectroscopic techniques such as ^{1}H NMR, ^{13}C NMR, and HRMS analyses. **PS-OMe** was further crystalized in DMF with the addition of a few drops of perchloric acid. The structure of **PS-OMe** was unambiguously confirmed from single crystal X-ray analysis as $C_{21}H_{17}ClO_7$ (Fig. S1†).

Photophysical properties

The absorption and emission spectra of **PS-OMe** and **PS-OH** in organic and aqueous solutions are shown in Fig. S2 and S3.† The absorption maximum (λ_{max}) at 505 nm of **PS-OMe** is shifted to (λ_{max}) 490 nm for **PS-OH** in chloroform which is attributed to a weak intramolecular charge transfer (ICT) from the donor to the acceptor pyrylium ring. The photophysical properties including maximum absorbance (λ_{max}), emission (λ_{max}), stokes shift, absolute quantum yield (Φ_F) and molar extinction coefficient (ε) are summarized in Table S1.† Both **PS-OMe** and **PS-OH** have higher Stokes shift when compared to fluorescein and rhodamine B, which can be an added advantage for imaging applications as it can help in setting filter and reduce autofluorescence (Table S2†). The solubility of **PS-OMe** and **PS-OH** in PBS buffer (pH 4) was found to be excellent as it shows a linear increase in absorbance till 55 μM and 80 μM for **PS-OMe** and **PS-OH** respectively (Fig. S4 and S5†). Subsequently, the absorption and emission spectra were measured with varying pH values in the buffer solution. At first, we checked the pH response of the control molecule, **PS-OMe**. At pH 4, the molecule exhibited a λ_{max} at 490 nm with a high molar absorptivity ($\varepsilon = 1.17 \times 10^4$ L mol^{-1} cm^{-1}) and exhibited an emission maximum at 560 nm with a 2551 cm^{-1} Stokes shift. With an increase in pH up to 8, there was no shift in either the absorbance or the emission maximum (Fig. S6†).

The maximum absorbance of **PS-OH** at 460 nm was gradually decreased with increasing pH and a new maximum at 570 nm appeared, indicating the deprotonation of the phenolic –OH (Fig. S7†). In the acidic pH, **PS-OH** exhibited an intense yellow fluorescence at 560 nm with a large Stokes shift (3882 cm^{-1}) in the acidic region and became almost non-fluorescent at normal physiological pH (pH 7.4). The gradual decrease of the fluorescence intensity with increasing pH from 4 to 7.4 indicates the potential of **PS-OH** for monitoring apoptosis. Above pH 8, a new peak with a maximum at 640 nm appears which is very weak when compared to the 560 nm emission (Fig. 2a).

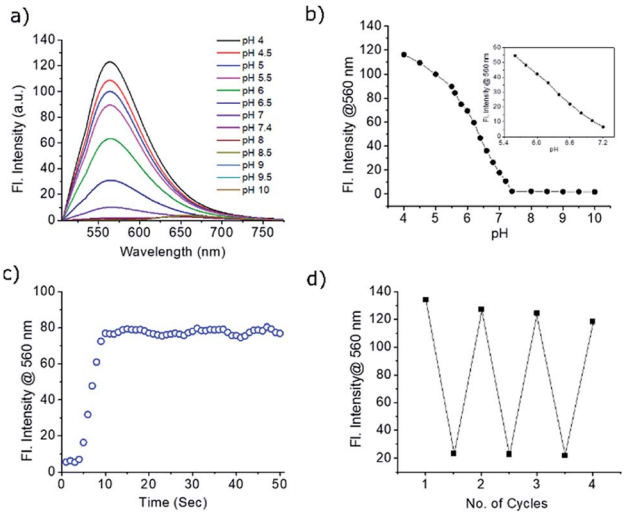

Fig. 2 (a) Fluorescence response of the probe **PS-OH** (20 μM) in PBS buffer at different pH ranging from 4 to 10. (b) Changes in the fluorescence maximum at 560 nm at different pH. Inset: linear variation of fluorescence intensity with pH between 5.6 and 7.2. (c) Response time of **PS-OH** upon addition of TFA (20 μL). (d) Reversibility in the fluorescence switching of the probe **PS-OH** between pH 4 and 7.4.

For a better insight on the "turn on" emission of **PS-OH**, the frontier orbital energy calculation was performed. The ground and excited state properties of **PS-OH** and the mono deprotonated **PS-OH** have been studied by using time-dependent density functional theory (TD-DFT) at the B3LYP/6-31G level using the Gaussian 16 program and compared with experimental absorption and emission spectra. The calculated absorption and emission spectra of **PS-OH** were well correlated with the experimental results (Fig S8†). However, after deprotonation, structural optimizations and subsequent frequency calculations revealed that a mixed state electronic transition from the unsymmetrical highest occupied molecular orbital (HOMO) to the symmetrical lowest unoccupied molecular orbital (LUMO) and LUMO+1 also correlates with the absorption bands. Due to a mixed excited state, there are at least two emissions with very minimum oscillator strength (f) indicating the non-emissive nature of **PS-OH** under neutral to basic conditions.

pH monitoring and imaging

The pK_a of **PS-OH**, calculated from the fluorescence titration curve using nonlinear regression by fitting the Boltzmann function was found to be 6.2 ± 0.03 (Fig. 2b). The emission intensity showed good linearity ($R^2 = 0.9962$) from pH 7.2 to 5.6 with a 48-fold enhancement, as shown in Fig. 2b (inset). Interestingly, the decrease of pH by 0.4 unit from normal cellular pH 7.4, enhanced the fluorescence intensity by 5.5-fold. Thus, even a minute fluctuation of the pH of a normal cell can be monitored with **PS-OH**.

For monitoring the dynamic pH change, a molecule should respond quickly towards pH variation, have good reversibility and photostability. The response of **PS-OH** was very fast towards

H^+, as it reaches a maximum fluorescence intensity within 9 s from pH 7.4 upon addition of trifluoroacetic acid (20 μL) (Fig. 2c). The retention of fluorescence intensity after four cycles between pH 4 and 7.4 (Fig. 2d) indicates that **PS-OH** is a good candidate for monitoring dynamic pH changes in the cellular system. The absolute quantum yields in the PBS buffer of pH 4 and 7.4 were found to be 0.11 and 0.03 respectively. In addition, photostability of **PS-OMe** and **PS-OH** was compared with rhodamine B and fluorescein by irradiation with a 200 W mercury lamp using a 455 nm long pass filter for 60 min. **PS-OMe** and **PS-OH** showed stability similar to rhodamine B and better than fluorescein (Fig. S9†).

The selectivity of the **PS-OH** towards different biologically relevant analytes including metal ions (Na^+, K^+, Ca^{2+}, Al^{3+}, Mg^{2+}, Zn^{2+} and Fe^{3+}), anions (AcO^-, OH^-, and OCl^-), reactive oxygen species (H_2O_2 and O_2^-), biothiols (Cys and GSH) and H_2S at pH 4 and 7.4 was tested. None of the analytes interfered with the fluorescence property of **PS-OH** (Fig. S10 and S11†). The observation indicates the potential for further exploring the response of **PS-OH** as a pH probe in live cells. The cytotoxicity of the probe using the human lung adenocarcinoma cancer cell line A549 was checked by incubating with **PS-OH** up to 10 mM concentration for 48 h. More than 90% cells were unaffected indicating the excellent biocompatibility of the probe (Fig. S12†). Also, the photobleaching of **PS-OMe** in the cell was compared with Mitotracker green and Lysotracker red. From the fluorescence intensity data, we could clearly see a comparable stability with Mitotracker green but less stability when compared to Lysotracker red (Fig. S13†).

Owing to the high turn-on sensitivity at acidic pH and good biocompatibility, the probe was used to investigate the intracellular pH response in the A549 cell line. At pH 7.4, there was almost no fluorescence observed with a green emission filter at 20 μM **PS-OH**. Nigericin was used to maintain the pH equilibrium between cells and the medium. With a decrease in pH to 7, a detectable fluorescence signal was observed (Fig. 3a). On further decrease of the pH, the intensity of fluorescence increased gradually (Fig. 3b). The fluorescence intensity obtained from the cells was plotted against pH which shows a good co-linearity with the photophysical data.

The quantitative data of the fluorescence response towards pH imbalance in live cells indicates the efficacy of the probe in cell imaging. Thus, **PS-OH** can be used to quantitatively determine the pH of the cell depending on its fluorescence response (Fig. 3c).

Various anticancer drugs and apoptotic agents target cells in different signalling pathways, varying the pH in each case. For example, it is reported that lipopolysaccharide (LPS) decreases intracellular pH (pH_i) to around 6,[20] and cisplatin induces only a slight decrease in pH_i of the cytoplasm,[21] whereas Mdivi-1 causes apoptosis *via* mitochondrial hyperfusion which does not acidify the cell cytoplasm.[22] We tried to evaluate pH imbalance by using the new probe during the treatment of these anticancer drugs or apoptotic agents. Cells were first incubated with **PS-OH** ($c = 20$ μM) for 10 minutes, followed by the treatment of Mdivi-1 (100 μM) LPS (1 μg mL^{-1}), and cisplatin (10 μM) separately for 12 h. The fluorescence images of cells were

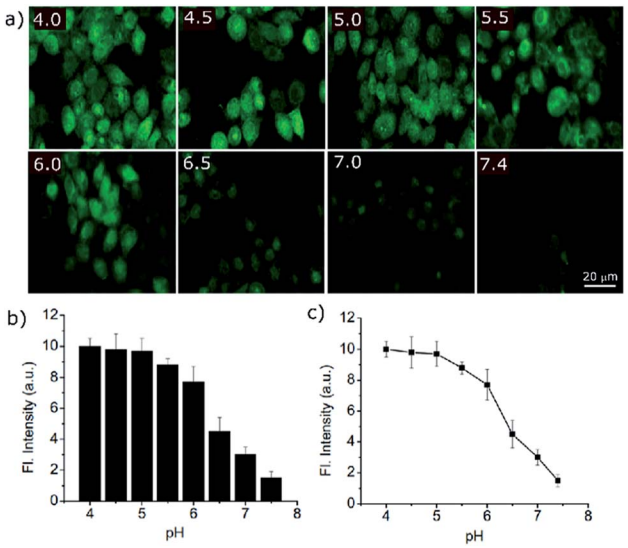

Fig. 3 (a) Fluorescence imaging of A549 cells after 10 min incubation with PS-OH (20 μM) in buffer solutions of different pH, in the presence of 10 μM nigericin. (b) A plot showing intensity of fluorescence obtained from the intracellular imaging at different pH. (c) Intracellular pH calibration curve of PS-OH obtained from the normalized intensity of fluorescence obtained from the cells at different pH.

analysed and it was found that in the case of Mdivi-1, there was no detectable change in fluorescence intensity (Fig. 4a–c). However, in the case of cisplatin, there was a slight change owing to minute acidification of the cells (pH ~ 6.49) compared to that of the control (pH ~ 7) (Fig. 4g–i), and for LPS treatment, the fluorescence intensity was significantly increased and the

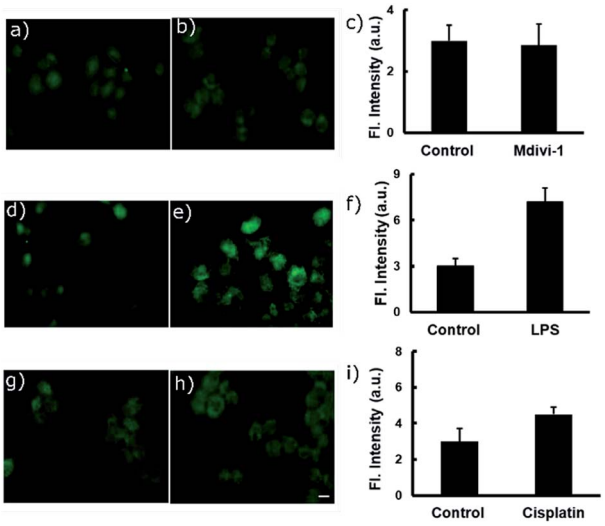

Fig. 4 Fluorescence imaging of A549 cells after treatment with different anti-cancer drugs and apoptotic agents. In each case, two sets of A549 cells were taken and incubated with 20 μM of PS-OH for 20 min. Then, one set of cells was kept as the control (a, d, g) and other sets were treated with (b) Mdivi-1, (e) LPS and (h) cisplatin respectively, for 12 h. The final fluorescence intensities of the control and treated cells were calculated (c, f, i) and compared with the calibration curve in Fig. 3c. Scale 20 μm.

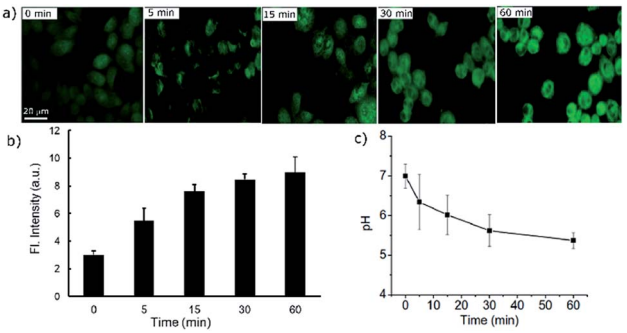

Fig. 5 (a) Real time fluorescence imaging of A549 cells stained with the probe **PS-OH** (20 μM) up to 60 minutes after treatment with 500 μM H_2O_2. (b) A plot of the fluorescence intensity with time during apoptosis. (c) Quantification of the corresponding dynamic changes in pH at different time points in comparison with the calibration curve in Fig. 3c.

final pH was found to be ~6.07 (Fig. 4d–f). These results show a very good agreement with the previous reports,[20–22] underlining the sensitivity and applicability of the new probe for the pH monitoring of cellular environments after chemotherapy.

Dynamic pH change monitoring with a molecular probe is undoubtedly an important aspect of cancer treatment modality. Thus, we investigated how the new probe can monitor the dynamic pH change in cells during apoptotic treatment. For this purpose, H_2O_2 was chosen as a reactive oxygen species which causes rapid cell death.[23,24] In the selectivity test, we have found that H_2O_2 does not affect the fluorescence response directly. Therefore, initially the cells were treated with the probe **PS-OH** for 10 min and then 500 μM of H_2O_2 was added to the medium. At 0, 5, 15, 30 and 60 min, fluorescence images were taken (Fig. 5a). An obvious increase in fluorescence was found within 5 min. With increase in time, the intensity further increased which is attributed to the continuous pH_i value decrease of the cells (Fig. 5b). This result proves the capability of the probe in monitoring the dynamic cellular pH change. From the previously calibrated graph, we could quantify the pH change at each time point (Fig. 5c).

Conclusions

In conclusion, we have established a new synthetic protocol to prepare a "core scaffold" of a pentacyclic pyrylium dye **PS-OMe**. A mechanistic understanding of the reaction pathways helped to establish an alternate efficient synthetic protocol of **PS-OMe** with nearly 70% yield. The pyrylium fluorescent probe **PS-OH** exhibited an 'on–off' response against the pH variation in cells during apoptosis. The strong acceptor at the centre ring of pyrylium, connected through two hydroxyl groups is the key to the bright fluorescent dye with excellent photophysical properties, including photostability, high molar absorptivity and large Stokes shifts. **PS-OH** exhibited an exceptional 'turn-on' pH response in the window of biological relevance both in solution state and in live cells. The new probe is capable of monitoring even a minute change of physiological pH (7.4) in cells during the therapeutic process with chemo drugs or apoptotic agents in real time.

Conflicts of interest

There are no conflicts to declare.

Acknowledgements

A. A. is thankful to the DST-SERB, Govt. of India for a J. C. Bose National Fellowship (SB/S2/JCB-11/2014). A. S. is grateful to the DST-SERB, Govt. of India, for a Ramanujan Fellowship (SB/S2/RJN148/2015). AcSIR Ph.D. student S. C. thanks DST-INSPIRE for a research fellowship. M. M. J. thanks the DST-SERB, Govt. of India for the National Post-Doctoral Research Fellowship (PDF/2016/001391). K. K. M. thanks the CSIR-FTT project (MLP0027, No. 33/Healthcare/FTT/2018(MT)). S. G. is thankful to the facility of Super Computer System, Institute for Chemical Research, Kyoto University, Japan.

References

1 (*a*) M. Mahmoudi, H. Hosseinkhani, M. Hosseinkhani, S. Boutry, A. Simchi, W. S. Journeay, K. Subramani and S. Laurent, *Chem. Rev.*, 2011, **111**, 253–280; (*b*) A. V. Naumova, M. Modo, A. Moore, C. E. Murry and J. A. Frank, *Nat. Biotechnol.*, 2014, **32**, 804–U121.

2 E. I. Dumbrava and F. Meric-Bernstam, *Cold Spring Harbor Mol. Case Stud.*, 2018, **4**, a001578.

3 (*a*) S. M. Barbon, V. N. Staroverov and J. B. Gilroy, *J. Org. Chem.*, 2015, **80**, 5226–5235; (*b*) E. Benedetti, L. S. Kocsis and K. M. Brummond, *J. Am. Chem. Soc.*, 2012, **134**, 12418–12421; (*c*) A. N. Butkevich, M. V. Sednev, H. Shojaei, V. N. Belov and S. W. Hell, *Org. Lett.*, 2018, **20**, 1261–1264; (*d*) R. Greiner, D. S. Ziegler, D. Cibu, A. C. Jakowetz, F. Auras, T. Bein and P. Knochel, *Org. Lett.*, 2017, **19**, 6384–6387; (*e*) V. Jamsheena, R. K. Mishra, K. S. Veena, S. Sini, P. Jayamurthy and R. S. Lankalapalli, *ACS Omega*, 2018, **3**, 856–862; (*f*) E. Kim, M. Koh, B. J. Lim and S. B. Park, *J. Am. Chem. Soc.*, 2011, **133**, 6642–6649; (*g*) G. Li, M. Zhao, J. Xie, Y. Yao, L. Mou, X. Zhang, X. Guo, W. Sun, Z. Wang, J. Xu, J. Xue, T. Hu, M. Zhang, M. Li and L. Hong, *Chem. Sci.*, 2020, **11**, 3586–3591.

4 (*a*) J. Hou, W. X. Ren, K. Li, J. Seo, A. Sharma, X. Yu and J. S. Kim, *Chem. Soc. Rev.*, 2017, **46**, 2076–2090; (*b*) L. Lyniv and S. Kireeva, *Int. J. Cancer*, 2002, 146; (*c*) L. Y. Lin, J. J. Zhao, L. L. Zhang, Y. Huang, F. G. Ye and S. L. Zhao, *Chem. Commun.*, 2018, **54**, 9071–9074.

5 (*a*) P. Wong, C. Lee and I. F. Tannock, *Clin. Cancer Res.*, 2005, **11**, 3553–3557; (*b*) E. M. Kniep, C. Roehlecke, N. Ozkucur, A. Steinberg, F. Reber, L. Knels and R. H. W. Funk, *Invest. Ophthalmol. Visual Sci.*, 2006, **47**, 1185–1192; (*c*) T. Yamashiro, N. Watanabe and Y. Kobayashi, *Biochem. Pharmacol.*, 1997, **54**, 143–148; (*d*) S. Matsuyama, J. Llopis, Q. L. Deveraux, R. Y. Tsien and J. C. Reed, *Nat. Cell Biol.*, 2000, **2**, 318–325; (*e*) L. M. Yang, Y. Y. Chen, Z. Z. Yu, W. Pan, H. Y. Wang, N. Li and B. Tang, *ACS Appl. Mater.*

Interfaces, 2017, **9**, 27512–27521; (*f*) D. Lagadic-Gossmann, L. Huc and V. Lecureur, *Cell Death Differ.*, 2004, **11**, 953–961.

6 (*a*) J. Jo, C. H. Lee, R. Kopelman and X. D. Wang, *Nat. Commun.*, 2017, **8**, 3983; (*b*) A. Jiang, G. Chen, J. Xu, Y. Liu, G. Zhao, Z. Liu, T. Chen, Y. Lia and T. D. James, *Chem. Commun.*, 2019, **55**, 11358–11361; (*c*) M. Tian, C. Liu, B. Dong, Y. Zuo and W. Lin, *Chem. Commun.*, 2019, **55**, 10440–10443; (*d*) F. Yu, X. Jing and W. Lin, *Anal. Chem.*, 2019, **91**(23), 15213–15219.

7 (*a*) J. R. Casey, S. Grinstein and J. Orlowski, *Nat. Rev. Mol. Cell Biol.*, 2010, **11**, 50–61; (*b*) M. H. Lee, J. H. Han, J. H. Lee, N. Park, R. Kumar, C. Kang and J. S. Kim, *Angew. Chem., Int. Ed.*, 2013, **52**, 6206–6209; (*c*) Y. Ning, S. Cheng, J. Wang, Y. Liu, W. Feng, F. Li and J. Zhang, *Chem. Sci.*, 2019, **10**, 4227–4235.

8 E. Persi, M. Duran-Frigola, M. Damaghi, W. R. Roush, P. Aloy, J. L. Cleveland, R. J. Gillies and E. Ruppin, *Nat. Commun.*, 2018, **9**, 2997.

9 (*a*) P. Anees, K. V. Sudheesh, P. Jayamurthy, A. R. Chandrika, R. V. Omkumar and A. Ajayaghosh, *Chem. Sci.*, 2016, **7**, 6808–6814; (*b*) G. Saranya, P. Anees, M. M. Joseph, K. K. Maiti and A. Ajayaghosh, *Chem.–Eur. J.*, 2017, **23**, 7191–7195; (*c*) D. S. Philips, S. Sreejith, T. He, N. V. Menon, P. Anees, J. Mathew, S. Sajikumar, Y. Kang, M. C. Stuparu, H. Sun, Y. Zhao and A. Ajayaghosh, *Chem.–Asian J.*, 2016, **11**, 1523–1527; (*d*) P. Anees, J. Joseph, S. Sreejith, N. V. Menon, Y. Kang, S. Wing-Kwong Yu, A. Ajayaghosh and Y. Zhao, *Chem. Sci.*, 2016, **7**, 4110–4116; (*e*) N. Gupta, S. I. Reja, V. Bhalla, M. Gupta, G. Kaur and M. Kumar, *J. Mater. Chem. B*, 2016, **4**, 1968–1977; (*f*) S. I. Reja, M. Gupta, N. Gupta, V. Bhalla, P. Ohri, G. Kaur and M. Kumar, *Chem. Commun.*, 2017, **53**, 3701–3704.

10 (*a*) S. Modi, C. Nizak, S. Surana, S. Halder and Y. Krishnan, *Nat. Nanotechnol.*, 2013, **8**, 459–467; (*b*) R. Subiros-Funosas, V. C. L. Ho, N. D. Barth, L. M. Tapia, M. Pappalardo, X. Barril, R. Ma, C. B. Zhang, B. Z. Qian, M. Sintes, O. Ghashghaei, R. Lavilla and M. Vendrell, *Chem. Sci.*, 2020, **11**, 1368–1374; (*c*) S. Benson, A. Fernandez, N. D. Barth, F. Moliner, M. H. Horrocks, C. S. Herrington, J. L. Abad, A. Delgado, L. Kelly, Z. Chang, Y. Feng, M. Nishiura, Y. Hori, K. Kikuchi and M. Vendrell, *Angew. Chem., Int. Ed.*, 2019, **58**, 6911–6915.

11 K. Q. Qiu, L. B. Ke, X. P. Zhang, Y. K. Liu, T. W. Rees, L. N. Ji, J. J. Diao and H. Chao, *Chem. Commun.*, 2018, **54**, 2421–2424.

12 H. Lee, W. Akers, K. Bhushan, S. Bloch, G. Sudlow, R. Tang and S. Achilefu, *Bioconjugate Chem.*, 2011, **22**, 777–784.

13 (*a*) F. A. Scaramuzzo, A. G. Campo, C.-C. Wu, A. H. Velders, V. Subramaniam, G. Doddi, P. Mencarelli, M. Barteri, P. Jonkheijm and J. Huskens, *Chem. Commun.*, 2010, **46**, 4193–4195; (*b*) C. T. F. Salfeena, Basavaraja, K. T. Ashitha, V. Praveen Kumar, S. Varughese, C. H. Suresh and B. S. Sasidhar, *Chem. Commun.*, 2018, **54**, 12463–12466; (*c*) B. S. Sasidhar, C. T. F. Salfeena and A. Ajayaghosh, *Process for the preparation of pyrylium salts*, 2018, PCT/IN2018/050898; (*d*) N. Manoj, G. Ajayakumar, K. R. Gopidas and C. H. Suresh, *J. Phys. Chem. A*, 2006, **110**, 11338–11345; (*e*) J. R. Wilt, G. A. Reynolds and J. A. Van Allain, *Tetrahedron*, 1973, **29**, 795–803; (*f*) D. Basavaraja, D. Dey, T. L. Varsha, C. T. F. Salfeena, M. K. Panda and B. S. Sasidhar, *ACS Appl. Bio Mater.*, 2020, **3**(2), 772–778.

14 (*a*) D. Asanuma, Y. Takaoka, S. Namiki, K. Takikawa, M. Kamiya, T. Nagano, Y. Urano and K. Hirose, *Angew. Chem., Int. Ed.*, 2014, **53**, 6085–6089; (*b*) M. H. Lee, N. Park, C. Yi, J. H. Han, J. H. Hong, K. P. Kim, D. H. Kang, J. L. Sessler, C. Kang and J. S. Kim, *J. Am. Chem. Soc.*, 2014, **136**, 14136–14142.

15 B. Lin, L. Fan, J. Y. Ge, W. J. Zhang, C. H. Zhang, C. Dong and S. M. Shuang, *Analyst*, 2018, **143**, 5054–5060.

16 A. Baji, A. Gyovai, J. Wolfoling, R. Minorics, I. Ocsovszki, I. Zupko and E. Frank, *RSC Adv.*, 2016, **6**, 27501–27516.

17 A. Lilienkampf, M. P. Johansson and K. Wahala, *Org. Lett.*, 2003, **5**, 3387–3390.

18 G. Yin, T. Niu, Y. Gan, T. Yu, P. Yin, H. Chen, Y. Zhang, H. Li and S. Yao, *Angew. Chem., Int. Ed.*, 2018, **57**, 4991–4994.

19 H. Chen, Y. Tang, M. Rena and W. Lin, *Chem. Sci.*, 2016, **7**, 1896–1903.

20 Y. Y. Zhang, S. L. Li and Z. W. Zhao, *Anal. Chem.*, 2016, **88**, 12380–12385.

21 M. V. Shirmanova, I. N. Druzhkova, M. M. Lukina, V. V. Dudenkova, N. I. Ignatova, L. B. Snopova, V. I. Shcheslavskiy, V. V. Belousov and E. V. Zagaynova, *Sci. Rep.*, 2017, **7**, 8911.

22 W. Zhang, X. Wang, P. Li, H. B. Xiao, W. Zhang, H. Wang and B. Tang, *Anal. Chem.*, 2017, **89**, 6840–6845.

23 M. H. Lee, J. H. Han, J. H. Lee, N. Park, R. Kumar, C. Kang and J. S. Kim, *Angew. Chem., Int. Ed.*, 2013, **52**, 6206–6209.

24 L. Y. Lin, J. J. Zhao, L. L. Zhang, Y. Huang, F. G. Ye and S. L. Zhao, *Chem. Commun.*, 2018, **54**, 9071–9074.